Materials Science in Semiconductor Processing 93 (2019) 182–187

Contents lists available at ScienceDirect

Materials Science in Semiconductor Processing

journal homepage: www.elsevier.com/locate/mssp

Thermal annealing effects on the structural, magnetic and hyperfine properties of the Fe/SnO_2/Fe thin film deposited by RF sputtering method

F.F.H. Aragón[a,*], J.C.R. Aquino[a], J.D. Ardisson[b], J.A.H. Coaquira[a]

[a] Núcleo de Física Aplicada, Instituto de Física, Universidade de Brasília, Brasília, DF 70910-900, Brazil
[b] Centro de Desenvolvimento da Tecnologia Nuclear, CDTN, 31270-901 Belo Horizonte, MG, Brazil

ARTICLE INFO

Keywords:
Low dimensional structures
Polycrystalline deposition
Inorganic compounds
Magnetic materials
Thermal annealing
Hyperfine properties

ABSTRACT

In the present work, the effect of the post-deposition annealing process in an air atmosphere on the structural and magnetic properties of the ternary Fe/SnO_2/Fe thin film, deposited by the sputtering technique was reported. X-ray diffraction (XRD) pattern confirms the formation of alpha-iron, magnetite and tin dioxide phases in the as-deposited film. Meanwhile, after the thermal annealing, the formation of hematite and tin dioxide phases was determined. Magnetization (M) measurements reveal some features after the annealing: i) a reduction of the coercive field (H_C), which has been assigned to the presence of hematite, and ii) the transformation of alpha-iron/magnetite phases into the hematite phase in accordance with results obtained from XRD data analysis. Those results were also confirmed by room temperature Conversion electron Mössbauer spectroscopy (CEMS) measurements carried out using a ^{57}Co(Rh) source. Furthermore, the doublets of the CEMS spectrum of the as-deposited film (21%) has been assigned to the signal of Fe^{3+} and $Fe^{2.5+}$ (mixture of Fe^{3+} and Fe^{2+}) ions, which diffuse into the SnO_2 matrix. The spectral area of those doublets is clearly reduced to 3% after the thermal annealing. It suggests the migration of the Fe ions from the non-magnetic phase to the magnetic phase. On the other hand, CEMS spectrum of the as-deposited film carried out with using a ^{119m}Sn source is well modeled with a doublet and a sextet. The doublet was assigned to Sn^{4+} ions of the SnO_2 phase; meanwhile, the sextet was assigned to Sn^{4+} ions located at interstitial and/or substitutional sites of the alpha-iron/magnetite phases. Those tin ions sense the supertransferred hyperfine field from Fe neighbor. After the thermal annealing, the CEMS spectrum was well modeled with only a doublet related to SnO_2 phase, suggesting that the tin ions have been out diffused from the magnetic phase (alpha-iron and magnetite) and incorporate into the no magnetic o-SnO_2.

1. Introduction

Nowadays, the fabrication of multilayer films formed by ferromagnetic (FM) and oxide semiconductor materials has been received outstanding attention, due to the singular combination of their electric and magnetic properties, which are the key to the development of spintronic devices [1]. In this scenery, ferromagnetic α-Fe thin films are extensively used due to its high Curie temperature (T_C = 1043 K). Yuasa et al. showed that multilayer films of Fe/MgO/Fe show a giant room-temperature magnetoresistance due to the magnetic tunneling of electrons between the electrodes through the thin insulating layer [1], besides, Miyazaki et al. [2] have obtained a similar result in Fe/Al_2O_3/Fe. On the other hand, the possibility of using those multilayer films as gas sensors by using their magnetic properties instead of their conventional electrical properties has risen the scientific and technological interests in this kind of nanostructures [3]. This is due to the fact that by monitoring the magnetic response of these nanostructured materials to sense a specific gas flow, it is not needed electrical contacts anymore as in conventional gas sensors and simplifying their use [4]. Reports of the use of the magnetic response of Fe-doped SnO_2 [3] and hematite [5] to sense a hydrogen (H_2) gas has been demonstrated and it gives rise to the possibility of using these materials as a magnetic gas sensor. On the other hand, rutile-type SnO_2 (space group $P42/mnm$), and tetragonal litharge-SnO (space group $P4/nmm$), are the most known tin oxide phases produced in oxidizing environment. However, a previous research has reported the formation of a third phase, orthorhombic-SnO_2 phase (stable at high pressures [6]) which is also stable in thin films [7,8]. Those reports suggested that the stress between the film and substrate develops an analogous action of high pressure to stabilize the high-pressure phase. Besides, Lamelas et al. [9] reported the formation of the orthorhombic SnO_2 phase in films grown on Si [001] by a thermal annealing at 700ºC from the polycrystalline litharge-SnO. The

* Corresponding author.
E-mail address: ffharagon@gmail.com (F.F.H. Aragón).

https://doi.org/10.1016/j.mssp.2019.01.004
Received 7 November 2018; Received in revised form 28 December 2018
Available online 09 January 2019
1369-8001/

orthorhombic-SnO_2 phase transform to the cassiterite-SnO_2 phase at 1050ºC. The authors suggested that the SnO phase is needed to stabilize the orthorhombic SnO_2 phase. Moreover, it is interesting to note that the presence of oxygen vacancies, commonly found in tin oxide phases, could provoke SnO nucleates locally around oxygen vacancies, contributing to the stabilization of the orthorhombic SnO_2 phase as reported by Van Komen et al. [10] in M-doped SnO_2 (M = Cr, Fe, and Co) nanoparticles. SnO_2 with rutile-type structure is a wide band gap (~ 3.6 eV) n-type semiconductor which is widely studied due to its potential applications as a conventional gas sensor due to its high reactivity with environmental gases [11], catalyst [12], transparent electrode [5], and so on. Likewise, hematite (α-Fe_2O_3) has attracted much attention, due to its extraordinary chemical stability in an oxidative environment, favorable optical band gap (~ 2.2 eV), abundance and low cost. Moreover, hematite has been also studied as gas sensor [13,14]. Chen et al. [10] have shown that by combining these materials (α-Fe_2O_3/SnO_2), their sensing characteristics exhibit a dramatic improvement when compared to their individual constituents.

In the present work, we have studied the structural, magnetic and hyperfine properties of as-deposited and thermal annealed Fe/SnO_2/Fe films, deposited on glass substrate by RF sputtering method.

2. Experimental details

A thin film of three thick layers (Fe/SnO_2/Fe) was grown at room temperature by a radio-frequency (RF) magnetron sputtering technique. The base pressure of the sputtering system was ~ 4×10^{-6} mbar and the argon pressure during the sputtering was kept at 3.6×10^{-2} mbar, using the sputtering targets of Fe and SnO_2 disks onto 1×1 cm^2 glass. The measurement of the thicknesses was determined by cross-section scanning electron microscope (SEM) images. After the deposition, the as-prepared (AP) multilayer film was thermally treated at 500 °C by 2 h in an air atmosphere. Both samples were stored in a vacuum environment to avoid the natural oxidation process. The crystalline structure was determined by X-ray diffraction (XRD), using the commercial diffractometer (Rigaku, model Ultima IV), with Cu-Kα radiation. Room temperature magnetic hysteresis curves were carried out using a commercial vibrating sample magnetometer (VSM) (LakesShore, model 7404). The surface morphology was analyzed by SEM images and atomic force microscopy (AFM). Conversion electron Mössbauer spectroscopy (CEMS) was carried out with ^{57}Co and ^{119m}Sn sources. A thin α-Fe foil has been used for calibration and all spectra were computer fitted with the least-square fitting routine using the NORMOS program and assuming Lorentzian lineshapes.

3. Results and discussion

Fig. 1 shows the room temperature XRD patterns of the as-prepared (AP) and thermally annealed (TA) Fe/SnO_2/Fe multilayer thin films. The formation of alpha-iron (α-Fe) phase is clearly observed in the as-prepared sample. Magnetite (Fe_3O_4) and orthorhombic-SnO_2 (o-SnO_2) crystalline phases were also determined, evidenced by the (220) and (311) Bragg peaks of Fe_3O_4 and (111) of o-SnO_2. It is worth mentioning that the formation of a tetragonal SnO_2 phase is obtained when a single monolayer of SnO_2 is deposited using the same conditions. This result shows that the multilayer configuration (Fe/SnO_2/Fe) favors the formation of the o-SnO_2 phase, which seems to be driven due to the strain induced by the top and bottom layers of iron that is in agreement with the presence of Sn^{4+} ions determined before and after the thermal annealing as shown below. Moreover, the presence of a small amount of SnO cannot be ruled out, mainly in the as-deposited thin film, due to the detection limit of the Mossbauer spectroscopy and to the fact that the (101) Bragg peak of the SnO is very close to the (111) reflection of the orthorhombic-SnO_2 phase. The formation of the magnetite phase is expected to happen due to the oxidation of the iron layers during the deposition process. When the thermal annealing was carried out in air atmosphere an orange color film was obtained, which is a characteristic color of the hematite phase (see the inset in Fig. 1(c)), evidenced by XRD data analysis of this sample, which shows the presence of only hematite (α-Fe_2O_3) and o-SnO_2 crystalline structures.

In order to obtain structural information such lattice parameters (*a, b* and *c*) and mean grain size ($< D >$), the X-ray diffractions patterns were further analyzed by the Rietveld refinement method using the General Structure Analyses System (GSAS) software [15]. The parameters determined from the analyses are listed in Table 1. As can be seen, both α-Fe and magnetite were determined for the as-prepared

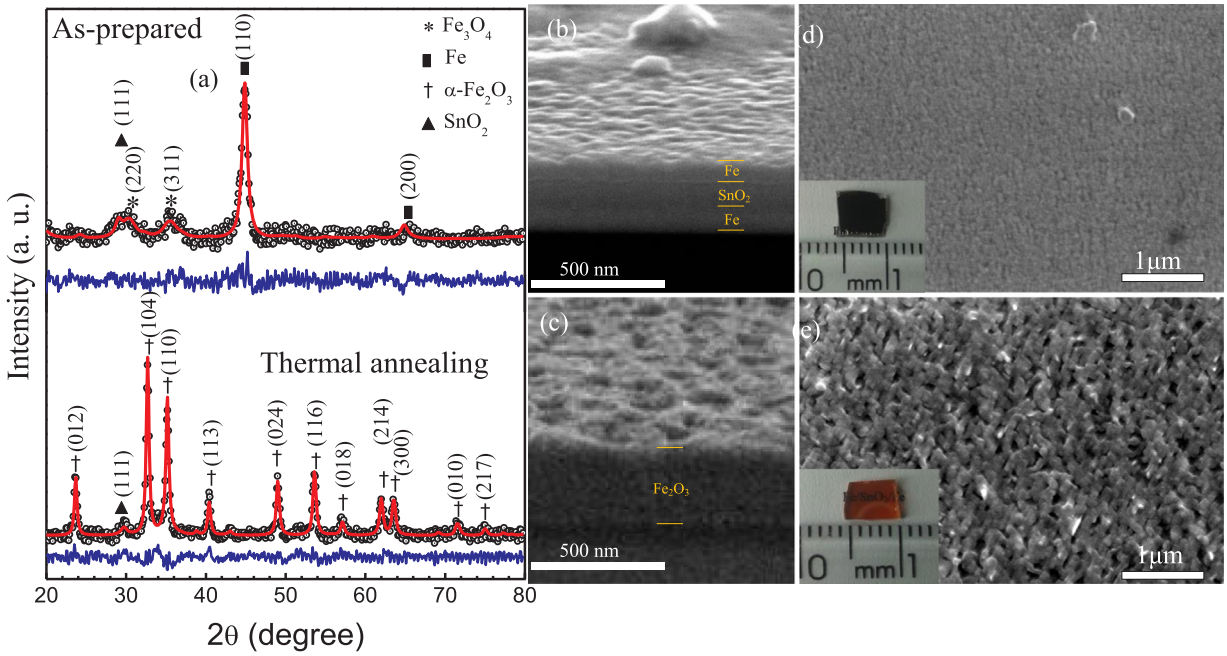

Fig. 1. (a) Room temperature XRD patterns of the as-prepared and thermal annealing Fe/SnO_2/Fe multilayer thin films. The observed and calculated data are represented by points and solid lines, respectively. The bottom solid line represents the difference between the observed and calculated data. (b) Cross-section SEM images for the as-prepared and (c) annealed thin film, (d) and (e) SEM images for the as-prepared and thermally treated multilayer thin films, respectively.

Table 1
Structural parameters obtained from the Rietveld refinement of XRD data, $S = R_{Exp}/R_{Wp}$ is a value that quantifies the quality of the refinement.

Sample	Phase	a (Å)	b (Å)	c (Å)	$< D >$ (nm)	S
AP	Fe	2.907	2.907	2.907	8(2)	1.28
	Fe_3O_4	8.568	8.568	8.568	4(2)	
	o-SnO_2	4.976	5.933	5.679	10(2)	
TA	α-Fe_2O_3	5.035	5.035	13.749	18(2)	1.24
	o-SnO_2	4.650	5.752	5.164	30(2)	

multilayer thin film. Those phases were transformed to the hematite phase when the film was subjected to a thermal annealing process. Larger lattice constants values in both phases (α-Fe and magnetite) were obtained when there are comparing to the literature values reported for bulk systems (a_{bulk} = 2.867 Å for α-Fe [16], and a_{bulk} = 8.396 Å for magnetite [17]). This fact could be associated with the strain states or even due to the presence of tin ions in those phases, which could drives to larger lattice constants due to the larger size of the tin ions. The relative change in the lattice constants ($\Delta a/a = (a - a_{bulk})/a \times 100\%$) were determined to be ~1.4 and ~2.0% for the cubic α-Fe and magnetite phases, respectively. The mean grain size values ($< D >$) listed in Table 1 were estimated assuming the diffraction peaks with a Lorentzian shape and using the Scherrer's relation: $< D > = K\lambda/\beta_{size} \times cos\Theta$, where $K = 0.9$ (spherical shaped crystals), λ is the X-ray wavelength (1.5418 Å for *Cu* K_α), β_{size} is the full width at half-maximum (*FWHM*) of the reflection, and θ is the diffraction angle. As observed in Table 1, the $< D >$ increases with the annealing process. This result is expected and it is correlated with the coalescence of smaller crystals into larger ones. This result is further verified by the increase in mean crystallite size of the o-SnO_2 phase, which does not suffer oxidation or phase change with the annealing. In order to determine the thickness of the films, cross-section SEM measurements were performed in both samples. For the as-deposited film (Fig. 1b), the top-Fe, SnO_2, and the bottom-Fe layer thicknesses are 60 ± 5, 103 ± 6 and 82 ± 4 nm, respectively. Furthermore, after the annealing (Fig. 2c) no multilayer was observed, evidencing the interdiffusion of the phases. An end thickness of 289 ± 21 nm is determined. This value is greater than the sum of the three thicknesses of as-deposited thin film. This has been assigned to the difference of densities between the α-Fe (7.9 g/cm^3), o-SnO_2(7.0 g/cm^3), with respect to the Fe_2O_3 (5.3 g/cm^3) phase.

In Fig. 1(d) and (e) is shown the SEM images carried out on the as-prepared and thermally treated multilayer thin films. As we can see, the surface morphology shows drastic changes promoted by the thermal annealing process with a clear increase in the mean grain size. On the other hand, the surface morphology was also analyzed by atomic force microscopy images (see Fig. 2), where it can be seen an increase in the average maximum height (Rz) and the average roughness (Ra) from Rz ~ 17.2 nm, Ra ~ 1.4 nm to Rz ~ 46.9 nm, Ra ~ 9.5 nm after the thermal annealing (both determined using the Gwyddion software [18]). From these results, we can infer that the annealing process favors the formation of higher structures and the rougher surface of the films, in agreement with the SEM images.

In Fig. 3 is shown the magnetic moment (M) as a function of the applied field (H) in the in-plane and out-of-plane configurations obtained for both samples, after the correction from the diamagnetic signal of the glass substrate. In the in-plane configuration, a noticeable decrease of ~89% of the magnetization saturation (MS) with the thermal annealing was determined, from 887 kA/m for the as-prepared film to 97 kA/m after the thermal annealing. Furthermore, the obtained MS ~ 887 kA/m value is lower than the one reported for Fe thin film (1480 KJ/Tm^3 [19]). This fact was assigned to the presence of the iron oxide phase and some iron atoms diffused to the tin oxide layer, in agreement with the Mössbauer spectroscopy results. Moreover, the M_S value after the thermal annealing (~ 97 kA/m) was associated with the oxidation of the iron metal, in agreement with the phase transformation from α-Fe/Fe_3O_4 to hematite, as determined from the XRD data analysis. This Ms value is between the ~ 2 kA/m and 380 kA/m reported for α-Fe_2O_3 and γ-Fe_2O_3, respectively [20]. As hematite phase is expected after the annealing, the obtained value could be associated to the presence of Sn ions in the hematite phase, which can generate an uncompensated ferromagnetic contribution due to the presence of nonmagnetic ions. The *M vs. H* curve of the as-prepared multilayer thin film obtained in the out-of-plane configuration exhibit a thinning (see inset of the Fig. 3), which could be associated with the two magnetic phases (magnetite and alpha-iron) with different magnetic coercivity. After the thermal annealing, the *M vs. H* curves show only single-hysteresis loops when the magnetic field is applied in both configurations. Besides, a clear reduction of the coercive field from ~ 209 to ~ 144 × 10^{-4} T is determined for the in-plane configuration and from ~ 407 to ~ 100 × 10^{-4} T for the out-of-plane configuration. This result can be attributed to the presence of only the *α-Fe_2O_3* as the magnetic phase in the annealed film. It is also observed, a clear reduction in the normalized remanence (*Mr/Ms*) from ~ 0.52 to ~ 0.25, for the in-plane configuration, after the annealing. On the other hand, the fact that the in-plane and out-of-plane curves for both films (as prepared and thermal annealed films) do not overlap each other with applied fields up to 1.5 T suggests that the in-plane magnetic anisotropy is stronger, as reported in the literature [21]. That magnetic anisotropy remains

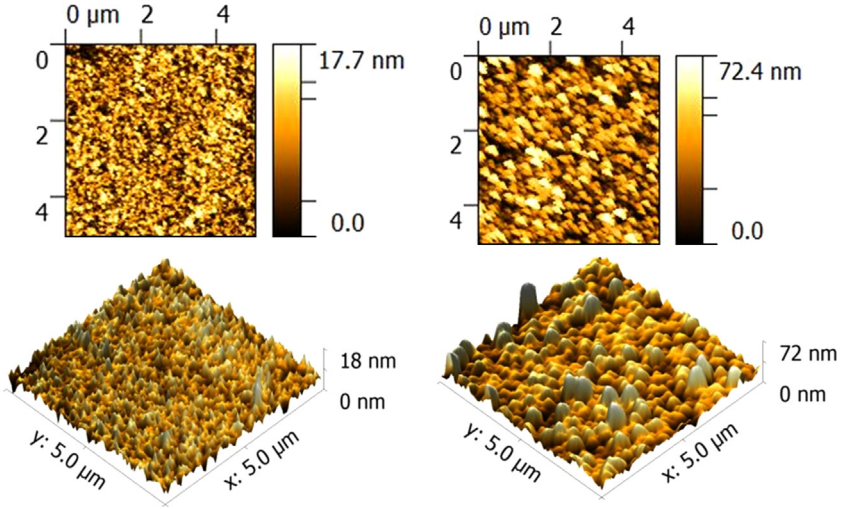

Fig. 2. AFM images. Left) for the as-prepared and Right) for the thermally annealed multilayer thin films.

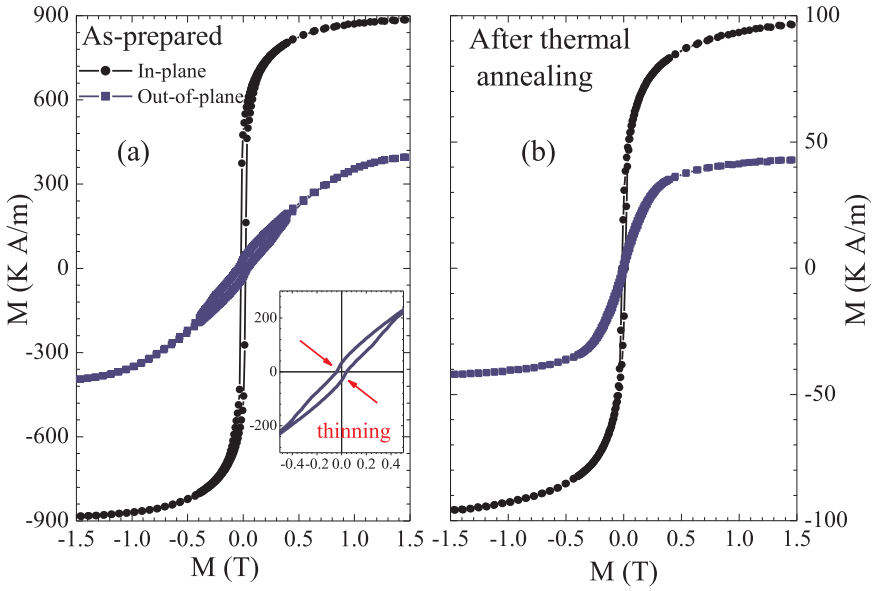

Fig. 3. Room-temperature magnetic hysteresis curves obtained for the (a) as-prepared and (b) thermal annealed *Fe/SnO₂/Fe* thin films. The magnetic field was applied parallel to the surface of the films (in-plane configuration) and perpendicular to film surface (out-of-plane configuration).

stronger even after the thermal treatment.

Room temperature CEMS measurements using ^{57}Co(Rh) source for both samples are shown in Fig. 4. The CEMS spectrum of the as-prepared film is well resolved using three sextets and two doublets. The list of the hyperfine parameters obtained from the fit, such as the isomer shift (*IS*), quadrupole splitting (*QS*) and hyperfine magnetic fields (B_{HF}) is presented in Table 2. The sextet I with a spectral area of 65% was assigned to the metallic α-Fe phase. Meanwhile, the other two sextets (II and III) with spectral areas of 6% and 8% were assigned to iron ions located in the tetrahedral $(Fe^{3+})_A$ and octahedral $(Fe^{3+}Fe^{2+})_B$ sites of the Fe_3O_4 phase. This is because of the expected hyperfine parameters for the tetrahedral and octahedral sites of Fe_3O_4 phase are in the range of $B_{HF}((Fe^{3+})_A) \approx 48.5–50.5$ T and $IS((Fe^{3+})_A) \approx 0.21–0.43$ mm/s, whereas for the octahedral site $B_{HF}((Fe^{3+}Fe^{2+})_B) \approx 46.5–45.3$ T and IS $((Fe^{3+}Fe^{2+})_B) \approx 0.63–0.75$ mm/s [22]. The two doublets were assigned to the signal of Fe^{3+} and $Fe^{2.5+}$ (mixture of Fe^{3+} and Fe^{2+}) ions diffused into the crystalline structure of SnO_2 phase and/or glass substrate [23,24]. On the other hand, when the thermal annealing was carried out, the Mössbauer spectrum shows drastic changes, which are in accordance with the structural characterization determined from XRD data analysis, as can be seen in Fig. 4. After the annealing, the CEMS spectrum was well fitted with only considering one sextet and one doublet. The hyperfine parameters of the sextet correspond to the hematite phase, which shows a spectral area of ~ 97%, whereas the doublet can be associated with the iron ions (Fe^{+3}) that remain in the crystalline structure of the SnO_2 phase [24].

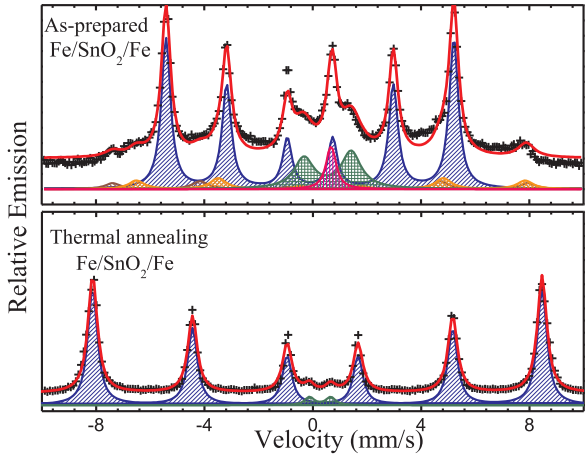

Fig. 4. Room-temperature conversion electron Mössbauer spectroscopy (CEMS) spectra of the as-prepared (AP) and thermal annealing (TA) $Fe/SnO_2/Fe$ films using ^{57}Co(Rh) source. The points represent the experimental data and the red line represents the calculated one. (For interpretation of the references to color in this figure legend, the reader is referred to the web version of this article).

In Fig. 5 are shown the room temperature ^{119m}Sn CEMS spectra for the as-prepared and thermally treated films. A preliminary analysis of the CEMS spectrum of the AP film indicates that the spectrum is well resolved by fitting with a doublet, which confirms the oxide state of tin (Sn^{4+}) in this sample. However, the linewidth of the spectrum (~ 1.2 mm/s) is broader when compared to that of the bulk SnO_2 [25], which suggests the likely occurrence of a distribution of quadrupole splitting (*QS*) in the AP film. The presence of a large number of doublets can be caused by several surroundings of tin ion induced by structural distortions in the *Sn* octahedral sites [26]. Nevertheless, as no clear evidence for the presence of Sn^{2+} is determined in both samples, the origin for the line broadening may be attributed not only to the quadrupole interactions, but also to a supertransferred hyperfine interaction (STHI) effect [27,28], associated to Sn^{4+} non-magnetic ions surrounded by Fe ions within the magnetic phase, which gives rise to the non-zero magnetic hyperfine field in the Sn nucleus. In this scenario, considering the likely occurrence of magnetic field felt by the nonmagnetic ^{119}Sn probes dispersed in the two Fe layers and considering that single SnO_2 films prepared by RF sputtering provide a thin linewidth component [25] the STHI effect is highly expected, and consequently the as-prepared thin film was fitted using a doublet and sextet distribution. The hyperfine parameters obtained from the fit for the doublet are $IS \approx 0.02$ mm/s, $QS \approx 0.54$ mm/s, and $\Gamma \approx 0.85$ mm/s are in agreement with the single SnO_2 thin film [25]. Furthermore, the magnetic sextet distribution has an average hyperfine magnetic field of $B_{HF} \sim 8.2$ T. This contribution has been assigned to the nonmagnetic Sn^{4+} ions surrounded by Fe ions. Those tin ions must be located in the interstitial and/or substitutional sites of α-Fe and Fe_3O_4 magnetic phase or, likely, in the interface region of the films. On the other hand, after thermal annealing, the spectral area of the doublet corresponding to the tin-ions (Sn^{4+}) of the SnO_2 phase is enhanced in detriment of the magnetic component observed in the as-prepared sample. The hyperfine parameters of the doublet became $IS \approx 0.49$ mm/s, $QS \approx 0.59$ mm/s and

Table 2
List of the hyperfine parameters obtained from the fit of room-temperature CEMS spectra. Isomer shift (*IS*), quadrupole shift (*QS*), hyperfine field (B_{HF}), line with (Γ) and the spectra area (A). The spectra were obtained using the ^{57}Co(Rh) source and the *IS* values are related to the *IS* of ∝-Fe.

Sample	Site	*IS* (mm/s) (± 0.08)	*QS* (mm/s) (± 0.08)	B_{HF} (T) (± 1)	Γ (mm/s) (± 0.08)	A (%) (± 2)	Assignment
AP	Sextet I	− 0.10	0.00	33	0.41	65	*α-Fe*
	Sextet II	0.28	0.00	48	0.60	6	$(Fe^{3+})_A$
	Sextet III	0.67	0.00	45	0.60	8	$(Fe^{3+}Fe^{2+})_B$
	Doublet I	0.12	0.68	–	0.40	16	Fe^{3+}
	Doublet II	0.55	1.74	–	0.88	5	$Fe^{2.5+}$
TA	Sextet	0.37	0.19	51	0.42	97	Fe_2O_3
	Doublet	0.37	0.78	–	0.40	3	Fe^{3+}

Note: The hyperfine parameters associated with Fe^{3+} ions are IS(Fe^{3+}) ≈ 0.15–0.434 mm/s, QS(Fe^{3+}) ≈ 0.161–1.106 mm/s, Fe^{2+}-ions IS (Fe^{2+}) ≈ 1.026–1.131 mm/s, QS(Fe^{2+}) ≈ 2.387–2.651 mm/s, and for the intermediate valence state + 2.5, IS($Fe^{2.5+}$) ≈ 0.653–0.793 mm/s, QS ($Fe^{2.5+}$) ≈ 1.479–1.763 mm/s [23].

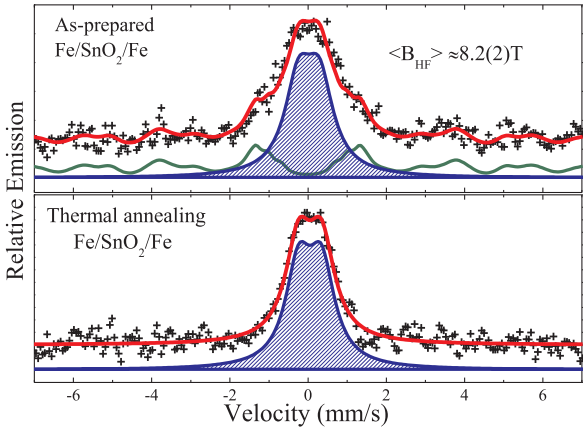

Fig. 5. Room-temperature conversion electron Mössbauer spectroscopy (CEMS) spectra of the as-prepared and thermally annealed *Fe/SnO$_2$/Fe* films obtained using ^{119m}Sn source. The points represent the experimental data and the red line represents the calculated data. (For interpretation of the references to color in this figure legend, the reader is referred to the web version of this article).

$\Gamma \approx 0.81$ mm/s after the annealing. The disappearance of the sextet after the annealing evidences the likely migration of the Sn ions occupying interstitial and/or substitutional sites of α-Fe and/or Fe_3O_4 magnetic phase to the SnO_2 phase.

4. Conclusion

In this work, we present the successful growth of the multilayer *Fe/SnO$_2$/Fe* thin film onto glass substrate. A morphologic characterization by SEM and AFM measurements indicates that the as-grown thin film shows a high crystalline quality and a good homogeneous surface, whereas the thermally treated thin film shows an increase in the surface roughness and larger mean grain size. Cross-section SEM images confirmed the formation the multilayer Fe/SnO2/Fe thin film with thicknesses of 60 ± 5, 103 ± 6 and 82 ± 4 nm, respectively. Moreover, after the thermal annealing, a single layer with a thickness of 289 ± 21 nm was determined. The clear thickness increase was associated with the Fe oxide phase formation; meanwhile, the multilayer destruction was assigned to the interdiffusion of the initial phases. The magnetization saturation (M_S = 887 kA/m) value is lower in comparison to that expected for α-Fe and it was associated with the presence of an iron oxide layer and iron atoms in the tin oxide phase. The saturation magnetization of the as-grown sample showed a decrease of ∼89% with the thermal annealing. This reduction was assigned to the presence of hematite phase. Results determined from conversion electron Mössbauer spectroscopy (CEMS) measurements using both ^{57}Co and ^{119m}Sn sources corroborate the formation of multilayer structure in the as-grown sample. Furthermore, CEMS measurements for the annealed sample confirm the formation of the hematite phase and suggest an interesting migration of Fe (Sn) ions from the non-magnetic (magnetic) to the magnetic (non-magnetic) phase induced by the annealing process.

Acknowledgments

The authors thank the Brazilian agencies CAPES, FAPEMIG, CNPq and FAPDF for financial support. The authors thank Dr. L.N. Coelho by the AFM measurements and the insightful comments of the manuscript.

References

[1] S. Yuasa, T. Nagahama, A. Fukushima, Y. Suzuki, K. Ando, Giant room-temperature magnetoresistance in single-crystal Fe/MgO/Fe magnetic tunnel junctions, Nat. Mater. 3 (2004) 868–871.
[2] T. Miyazaki, N. Tezuka, Giant magnetic tunneling effect in Fe/Al_2O_3/Fe junction, J. Magn. Magn. Mater. 139 (1995) L231–L234.
[3] A. Punnoose, K.M. Reddy, J. Hays, A. Thurber, M.H. Engelhard, Magnetic gas sensing using a dilute magnetic semiconductor, Appl. Phys. Lett. 89 (2006) 112509.
[4] A. Thurber, K.M. Reddy, A. Punnoose, Influence of oxygen level on structure and ferromagnetism in $Sn_{0.95}Fe_{0.05}O_2$ nanoparticles, J. Appl. Phys. 105 (2009) 07E706.
[5] A. Punnoose, K.M. Reddy, A. Thurber, J. Hays, M.H. Engelhard, Novel magnetic hydrogen sensing: a case study using antiferromagnetic haematite nanoparticles, Nanotechnology 18 (2007) 165502.
[6] K. Suito, N. Kawai, Y. Masuda, High pressure synthesis of orthorhombic SnO_2, Mater. Res. Bull. 10 (1975) 677–680.
[7] S. Kim, D.-H. Kim, S.-H. Hong, Epitaxial growth of orthorhombic SnO_2 films on various YSZ substrates by plasma enhanced atomic layer deposition, J. Cryst. Growth 348 (2012) 15–19.
[8] Z. Chen, J.K.L. Lai, C.-H. Shek, Facile strategy and mechanism for orthorhombic SnO_2 thin films, Appl. Phys. Lett. 89 (2006) 231902.
[9] F.J. Lamelas, S.A. Reid, Thin-film synthesis of the orthorhombic phase of SnO_2, Phys. Rev. B 60 (1999) 9347–9352.
[10] C.V. Komen, A. Thurber, K.M. Reddy, J. Hays, A. Punnoose, Structure–magnetic property relationship in transition metal (M=V,Cr,Mn,Fe,Co,Ni) doped SnO_2 nanoparticles, J. Appl. Phys. 103 (2008) 07D141.
[11] B. Bahrami, A. Khodadadi, M. Kazemeini, Y. Mortazavi, Enhanced CO sensitivity and selectivity of gold nanoparticles-doped SnO_2 sensor in presence of propane and methane, Sens. Actuators B 133 (2008) 352–356.
[12] A. Rabis, D. Kramer, E. Fabbri, M. Worsdale, R. Kötz, T.J. Schmidt, Catalyzed SnO_2 thin films: theoretical and experimental insights into fabrication and electrocatalytic properties, J. Phys. Chem. C 118 (2014) 11292–11302.
[13] K.G. Godinho, A. Walsh, G.W. Watson, Energetic and electronic structure analysis of intrinsic defects in SnO_2, J. Phys. Chem. C. 113 (2009) 439–448.
[14] A. Kay, I. Cesar, M. Gratzel, New benchmark for water photooxidation by nanostructured alpha-Fe_2O_3 films, J. Am. Chem. Soc. 128 (2006) 15714–15721.
[15] A.C. Larson, R.B. Von Dreele, General Structural Analysis System (GSAS), Los Alamos National Laboratory Report, LAUR, 2004, pp. 86–748.
[16] M. Polcarova, J. Zura, Method for determination of lattice-parameters on single-crystals, Czech J. Phys. 27 (1977) 322–331.
[17] P. Hu, S.G. Zhang, H. Wang, D.A. Pan, J.J. Tian, Z. Tang, A.A. Volinsky, Heat treatment effects on Fe_3O_4 nanoparticles structure and magnetic properties prepared by carbothermal reduction, J. Alloy. Compd. 509 (2011) 2316–2319.
[18] D. Nečas, P. Klapetek, Gwyddion: an open-source software for SPM data analysis, Cent. Eur. J. Phys. 10 (2012) 181–188.
[19] C. Gao, O. Brandt, H.-P. Schönherr, U. Jahn, J. Herfort, B. Jenichen, Thermal stability of epitaxial Fe films on GaN(0001), Appl. Phys. Lett. 95 (2009) 111906.
[20] S.M. Suturin, A.M. Korovin, S.V. Gastev, M.P. Volkov, A.A. Sitnikova, D.A. Kirilenko, M. Tabuchi, N.S. Sokolov, Tunable polymorphism of epitaxial iron oxides in the four-in-one ferroic-on-GaN system with magnetically ordered α-, γ-, ε-Fe_2O_3 and Fe_3O_4 layers, Phys. Rev. Mater. 2 (2018) 073403.
[21] A. Kalache, A. Markou, S. Selle, T. Höche, R. Sahoo, G.H. Fecher, C. Felser,

Heteroepitaxial growth of tetragonal $Mn_{2.7-x}Fe_xGa_{1.3}$ ($0 \leq x \leq 1.2$) Heusler films with perpendicular magnetic anisotropy, APL Mater. 5 (2017) 096102.
[22] J.G. Stevens, A. Khasanov, J.W. Miller, H. Pollak, Z. Li, Mössbauer Mineral Handbook, Mössbauer Effect Data Center, 2002.
[23] V. Coulibaly, J. Sei, S. Oyetola, M.T. Sougrati, J.C. Jumas, Asian J. Appl. Sci. 5 (2012) 460–472.
[24] Y. Wang, K. Nomura, X. Liu, A.I. Rykov, C. Jin, T. Liu, J. Wang, Structural and magnetic properties of ^{57}Fe-doped TiO_2 and ^{57}Fe/Sn-codoped TiO_2 prepared by a soft-chemical process, Eur. J. Inorg. Chem. 2016 (2016) 2131–2135.
[25] B. Stjerna, C.G. Granqvist, A. Seidel, L. Häggström, Characterization of rf-sputtered SnO_x thin films by electron microscopy, Hall-effect measurement, and Mössbauer spectrometry, J. Appl. Phys. 68 (1990) 6241–6245.
[26] F.H. Aragón, R. Cohen, J.A.H. Coaquira, G.V. Barros, P. Hidalgo, L.C.C.M. Nagamine, D. Gouvêa, Hyperfine Interact. 202 (2011) 73–79.
[27] J.Z. Jiang, R. Lin, S. Mørup, K. Nielsen, F.W. Poulsen, F.J. Berry, R. Clasen, Mechanical alloying of an immiscible α-Fe_2O_3-SnO_2 ceramic, Phys. Rev. B 55 (1997) 11–14.
[28] S. Constantinescu, L. Diamandescu, I. Bibicu, D. Tarabasanu-Mih Aila, M. Feder, ^{119}Sn- and ^{57}Fe- Mössbauer investigation of $xSnO_2$-[(1-x)[α-Fe_2O_3] nanoparticles system. (I) Magnetic hyperfine field distribution in Sn-low diluted system, Rom. J. Phys. 56 (2011) 692–707.